ATMOSPHERIC SCATTERING OF SONIC-BOOM INTENSITIES*

ROBERT DRESSLER

The Ford Motor Company, Scientific Laboratory
Dearborn, Michigan

AND

NILS FREDHOLM

The Aeronautical Research Institute of Sweden (FFA)
Stockholm, Sweden

INTRODUCTION

Variable atmospheric conditions of winds and temperatures can cause a significant scatter about average values for sonic-boom intensities at ground level. Furthermore, booms created by airplanes flying at high cruising altitudes are often sufficiently intense, even for statistically average conditions, to cause serious concern. It is therefore imperative to have some realistic quantitative knowledge about the magnitudes and frequencies of such scattering by wind-and-temperature variations to serve as a basis for intelligent planning and for a sensible policy regarding the future of commercial supersonic transportation.

There are many ways (other than the obvious factors of airplane size, Mach number, altitude, etc.) by which a big change can be created in sonic-boom intensity at ground level. Although this paper is restricted to just one important category, for proper perspective on the total problem the following table is included of some of the many possibilities which will require careful analysis. Here the x-axis is horizontal, taken along the

* The first portions of this paper were completed by Mr. Dressler during a one-year appointment at FFA.

flight path, y perpendicular to x, and z the upward vertical axis; A denotes general atmospheric properties, T temperature, W wind, and t time:

CONDITIONS FOR CHANGES IN BOOM INTENSITY

Steady conditions	Unsteady conditions
1. $A(z)$ only, not function of x, y, or t 1*a*. $T(z)$ and $W \equiv 0$ 1*b*. $T(z)$ and $W(z)$ 2. $A(y,z)$ 2*a*. $T(y,z)$ and $W \equiv 0$ 2*b*. $T(y,z)$ and $W(y,z)$	3. Flight maneuvers with: 3*a*. $T(z)$ and $W \equiv 0$ 3*b*. $T(z)$ and $W(z)$ 4. Constant, level flight with: 4*a*. $T(x,y,z,t)$ and $W \equiv 0$ 4*b*. $T(x,y,z,t)$ and $W(x,y,z,t)$ 5. Flight maneuvers with unsteady T and/or unsteady W

Analysis of case 1*a* by linear weak-shock theory is equivalent mathematically to ordinary geometrical-optics theory, with reciprocal of temperature analogous to index of refraction. This case has been subjected to considerable study by many investigators. Case 3*a* likewise has been studied by Rao [1], Randall [2], Lansing [3], Warren [4] and others. The case 1*b* is the subject of this paper; and by utilization of the computational procedures to be described, case 2*b* also could be analyzed without additional difficulties. The other possibilities tabulated above may present mathematical difficulties, and attempts at analysis have thus far not been made to our knowledge.

If a boom magnification or focus occurs within the "steady" categories, the afflicted ground area will extend over a relatively long path, parallel to the entire flight path, while the atmospheric conditions hold more or less constant. High-intensity areas in the "unsteady" categories will, however, be transient, probably affecting relatively limited ground areas.

A comprehensive study of sonic-boom magnifications can probably best be undertaken by mathematical methods rather than by experimental measurements, because of the extreme difficulty to position, in advance, a pressure-recording instrument in or near an area where a peak magnification will occur. There are so many parameters entering into this problem that it is practically impossible to guess in advance where to look for a magnification region. When just a few instruments are placed miles apart across a wide sonic-boom carpet, the peak reading among the measurements usually does not approximate the values attained in some small focal region which may exist as a narrow band somewhere between the instruments. Therefore, the totality of measured values taken to date on sonic-boom intensities probably does not give even a rough indication of

the scatter which may exist in the actual peak values of the disturbances. With a basis, however, of some 80 published experimental measurements (after normalizing these measurements for differences in altitude, Mach number, and other significant parameters), Lundberg [5] calculated a scatter measured by a standard deviation of 30 percent above the average values. The actual situation probably would exhibit an even larger scatter if these measurements had included the peak magnified intensities.

BASIC MATHEMATICAL THEORY

An airplane in a supersonic stream creates a complicated pattern of strong shocks and a nonlinear flow field. At a comparatively short distance away these combined effects merge to create the familiar Mach cone, which, as the exterior boundary of the disturbance, is a strong conical shock wave. However, the disturbance is rather quickly reduced at a distance away from the source, by viscous action and by geometrical expansion, so that it can then be regarded as a linear wave motion; and it takes on the form of the so-called "N-wave." The front and tail pressure jumps of this N-wave correspond to the original bow and tail shocks arising at the airplane.

The steady case 1b will be analyzed in this paper. A previous investigation of this case was made as part of the activities of the "Project Big Boom" in 1960, which included besides the mathematical calculations also experimental measurements. These were taken at four stations stretched across the flight path in Nevada. Results from the Project Big Boom ("PBB") have been reported by Reed [6,7], and by Reed and Adams [8]. The PBB calculations were made for Mach number $M = 1.5$, for a simple wind structure (constant direction, linear velocity from zero at ground to 200 knots at the 40,000 ft cruising altitude), and for a linear temperature distribution from $+20°C$ to $-50°C$ at these levels. Our initial calculations were made on the same atmospheric model (the PBB model), to serve as a check. Our results, however, disagree considerably with the PBB results because we have used the exact mathematical formulation for geometric acoustic propagation in winds, whereas the PBB calculations were based upon a simplified theory due to Rayleigh [9] which is not altogether applicable to sonic-boom calculation. This point will be discussed in detail in a later section.

We first give a brief outline of generalized geometrical acoustic theory (weak-shock theory) with winds. This serves as the basis for all of our calculations: In order to use the summation convention for repeated subscripts, we here denote (x,y,z) by (x_1,x_2,x_3). Let the moving surface formed

by a weak shock wave be given by $t = W(x_1,x_2,x_3)$; thus at any moment $t = t_0$ the shock surface in space is defined by the equation $t_0 = W(x_1,x_2,x_3)$. One then considers the normal direction to the wavefront given by grad W and introduces the "wave-normal vector" $\bar{p}$ defined as $\bar{p} = \text{grad } W$. The wind velocity vector is denoted by $\bar{u} = (u_1,u_2,u_3)$, and the scalar c denotes local sound speed and is a function of temperature. Starting from the basic equations of fluid dynamics and associated discontinuity conditions, the nonlinear partial differential equation for the unknown wavefront function W can be derived as

$$c^2(W_{x_j}) = (1 - u_jW_{x_j})^2 = 1 - 2u_iW_{x_i} + u_iu_jW_{x_i}W_{x_j} \tag{1}$$

which is the general "Eiconal" equation for geometrical acoustics. The three terms on the left side are the same as in the no-wind case, but the wind vector adds nine additional terms to the right-hand side compared with the simple Eiconal equation $c^2(W_{x_j})^2 = 1$ for geometrical optics or geometrical acoustics without winds. The wind velocity at any point may be subsonic, transonic, or supersonic with respect to the local c. In the supersonic case, two separate wavefronts exist (a fast branch and a slow branch). Further details can be found in Dressler [10] and a complete, rigorous derivation in Keller [11]. We let $\bar{\nu}$ denote the unit vector in the direction of $\bar{p}$, and $\bar{v}$ is the normal velocity of the wavefront at any point. It can be proved that

$$|\bar{v}| = \frac{1}{|\bar{p}|}$$

and (2)

$$|\bar{v}| = |\bar{u}| \cos\psi \pm c$$

where ψ is the angle between the directions of $\bar{p}$ and of $\bar{u}$. The + sign is taken for the subsonic, transonic, and fast-branch supersonic cases, and the − sign for the slow-branch supersonic case. When Eq. (1) is written as a partial differential equation in the quantities p_i

$$0 = c^2p_i^2 - (1 - u_jp_j)^2 \equiv \mathfrak{H}(x_1,x_2,x_3,W,p_1,p_2,p_3) \tag{3}$$

the Hamiltonian $\mathfrak{H}$ is independent of the function W explicitly, and is therefore already in "canonical form" (Courant-Hilbert [12]). Accordingly, for the "characteristic strips," the associated system of 6 ordinary differential equations (the Hamiltonian equations) which define the ray- and wave-normal directions is

$$\frac{dx_1(\sigma)}{d\sigma} = \frac{\partial \mathfrak{H}}{\partial p_1} = 2c^2 p_1 \pm 2c\sqrt{p_1^2 + p_2^2 + p_3^2}\, u_1$$

$$\frac{dx_2(\sigma)}{d\sigma} = \frac{\partial \mathfrak{H}}{\partial p_2} = 2c^2 p_2 \pm 2c\sqrt{p_1^2 + p_2^2 + p_3^2}\, u_2$$

$$\frac{dx_3(\sigma)}{d\sigma} = \frac{\partial \mathfrak{H}}{\partial p_3} = 2c^2 p_3 \pm 2c\sqrt{p_1^2 + p_2^2 + p_3^2}\, u_3 \tag{4}$$

$$\left.\begin{aligned} \frac{dp_1(\sigma)}{d\sigma} &= -\frac{\partial \mathfrak{H}}{\partial x_1} = \\ \frac{dp_2(\sigma)}{d\sigma} &= -\frac{\partial \mathfrak{H}}{\partial x_2} = \\ \frac{dp_3(\sigma)}{d\sigma} &= -\frac{\partial \mathfrak{H}}{\partial x_3} = \end{aligned}\right\} \text{dependent upon given forms of } c(x_i) \text{ and } \bar{u}(x_i)$$

where σ is any parameter as independent variable, $x(\sigma)$ any ray, and $\bar{p}(\sigma)$ its associated wave-normal vector. The rays are the projections into the (x_i) 3-space of the "characteristic lines" of the original partial differential equation in the (x_i, W) 4-space. The $-$ sign is taken only for the slow-branch supersonic case.

One notes immediately that in the trivial case when c and $\bar{u}$ are constant throughout the medium, then $\bar{p}$ is constant. Hence the $dx_i/d\sigma$ quantities, which define the tangent direction to the rays, are constant, and thus the rays are straight lines, and wave-normal directions are constant.

Since the coefficients in the first three equations of (4) are scalars, it follows that:

(a) If $\bar{u} \equiv 0$, then the ray is parallel to $\bar{p}$.
(b) If $\bar{u}$ is parallel to $\bar{p}$, then the ray is parallel to $\bar{p}$.

In all other cases the rays and wave-normals will have *different* directions at each point. It was for the purpose of emphasizing these relations (a) and (b) that the brief sketch of geometrical-acoustic theory was introduced. These relations show that ray directions and wave-normal directions will approximately coincide *only if* the wind velocities are small (relative to c) and/or if the wind direction is *only slightly* inclined to the wavefront normals. Conversely, *when wind velocities are large and wavefront directions are obliquely inclined to the wind, the directions of rays and wave normals will diverge considerably; then a careful distinction must be made between ray directions and wave-normal directions, as wavefronts are no longer almost perpendicular to the rays.*

When the parameter σ is suitably scaled, the first three equations of (4) can be written in the form

$$\frac{d\bar{x}}{d\sigma} = \pm c\bar{\nu} + \bar{u} \tag{5}$$

Equations (2) and (5) proved as indicated are the fundamental relations governing the behavior of acoustic propagation in winds. These were taken as basic assumptions rather than as provable relations by Milne [13] in what was probably the first paper to develop the full mathematics governing acoustic propagation in strong winds.

To summarize, it is thus seen that the two important atmospheric parameters affecting sonic-boom propagation are temperature distributions and wind distributions. In linear geometrical-acoustic theory the temperature variation, through its effect on local sound speed, is strictly analogous to the reciprocal of index of refraction in geometrical optics, and thus introduces no complexities into the calculations. Winds, however, have the combined effects of introducing nonisotropy into the propagation medium and also of introducing convection, thus adding in general the many extra terms to the basic mathematical expressions. The winds cause acoustic wave fronts to be inclined obliquely to the acoustic rays; the simple orthogonality relation between these directions no longer prevails.

Since we neglect dissipative mechanisms such as viscosity in this theory, and since the rays as characteristics define the subsequent path of an initial disturbance, it can be shown that acoustic energy in winds must still be conserved along a "ray tube," just as in the simpler theory. To solve a sonic-boom propagation problem, therefore, it is only necessary to calculate the six unknowns defining the rays and wave-normals.

INTEGRATION METHODS FOR RAYS AND WAVEFRONTS

SOLUTION BY HAMILTONIAN EQUATIONS

For numerical solutions we favor the Runge-Kutta 4th order integration method applied to Eq. (4). Initial conditions to start the computations along any ray consist of the six quantities $x_i(\sigma_0)$ and $p_i(\sigma_0)$ for initial position of the ray and initial wavefront orientation. After a system of rays has been calculated, relative energy intensities may be obtained by utilization of the ray-tube energy conservation law.

Although system (4) is in general too complicated to permit analytic (non-numerical) solutions, we have found one nontrivial exact solution of Eq. (4) for the case of a sonic boom with a linearly varying wind velocity, for a crosswind direction. Details of this solution can be found in Dressler

[10]. By comparing our numerical integration results against this exact solution, we have been able to determine the required magnitudes of integration intervals so that our numerical results will contain errors less than 0.1 percent.

Although we recommend integration of the system (4) for the analysis of more complicated cases such as $2b$ listed in the preceding table, for atmospheric conditions $A(y,z)$ which might occur when a flight path is taken parallel to a mountain range or to a seacoast or lakecoast, for the simpler case $1b$ which we are here analyzing it is slightly faster to calculate the rays and wave-normals by direct application of a generalized Snell's law. In all of our following calculations, we have therefore used the Snell's law approach:

SOLUTION BY SNELL'S LAW

Alternatively, instead of integrating Eq. (4) directly, one can calculate, after dividing the medium into piecewise-constant thin layers for temperature, wind magnitude, and direction, by applying Snell's law for the refractive behavior at the discontinuities at each interface together with the known solutions (straight-line rays and constant wave-normal directions) within each layer.

Snell's law is merely a condition along an interface expressing continuity between an incident wavefront, the refracted wavefront, and the reflected wavefront. From the requirement that these wavefront hypersurfaces in x, y, z, t space should join together continuously, with no time-delay, where they intersect the (stationary) hypersurface of the interface, elementary vector analysis yields Snell's law for acoustic behavior in winds:

$$\frac{\sin \theta_I}{|\bar{v}_I|} = \frac{\sin \theta_T}{|\bar{v}_T|} = \frac{\sin \theta_R}{|\bar{v}_R|} \tag{6}$$

for the three wavefronts, where $\theta_I(\theta_T$ or $\theta_R)$ is the angle between the wave-normal direction, given by $\bar{p}_I(\bar{p}_T$ or $\bar{p}_R)$, of the incident (transmitted or reflected) wavefront and the direction N normal to the interface across which jumps in temperature and winds may occur. The relation in Eq. (6) for the reflected waves is ignored in the calculations; it is consistent with the geometrical-acoustics approximation to neglect reflected waves, except in the case of total reflection, since in the limit for very thin layers and hence small jumps in c and $\bar{u}$, the amplitudes of the reflections die out sufficiently rapidly, as indicated by the Fresnel formulas.

It should be emphasized that there is no reference in Eq. (6) to the rays; only the wave-normal directions are involved together with the wave-normal velocities. The wind effect enters through the anisotropic behavior

of the wave-normal velocities, which are thus functions of the angle θ_I and the unknown angle θ_T, as indicated by Eq. (2). The rays are used only to fix the position at each interface where the next application of Snell's law is to be made.

It might appear from the elementary form of Eq. (6) that there is no difference here from the simple no-wind theory, but after replacement of $\bar{v}$ by Eq. (2) and some vector calculations, the generalized Snell's law with winds for the wave-normal directions takes the form for passage from the nth to the $(n - 1)$th layer,

$$\sin \theta_{n-1} = \frac{c_{n-1} \sin \theta_n}{| \bar{v}_n | - \bar{u}_{n-1} \bar{v}_n} \tag{7}$$

APPLICATION TO SONIC-BOOM PROPAGATION

Two possible formulations exist within this theory for sonic-boom calculations. (a) Either the airplane source may be considered as fixed in space in a moving stream, consisting of the supersonic mainstream determined by Mach number, plus the added variable subsonic winds, or (b) the airplane source may be considered as moving at the Mach number of the flight in a medium consisting only of the variable subsonic winds. Formulation (a) might lend itself more easily to calculations for the interior disturbance within the shock envelope, and would include a "double" ray system, but (b) permits the calculations for intensities just *at* the Mach cone (corresponding only to the initial pressure rise at the beginning of the N-wave) to be performed with some simplification. As the airplane moves, at each moment a wavefront originates at the moving source. These propagate in the winds as distorted spheres forming a distorted Mach cone as their envelope. Disregarding the internal disturbance, the envelope of wavefronts (Mach cone) may be considered as the only wavefront of interest, thus attention need be given only to the subset of rays and wave normals associated with this envelope. This procedure is rigorously justified, for example, in Warren and Randall [14], and was employed also in the PBB calculations [6]; it is altogether sufficient for a study of changes in sonic-boom intensity.

Let $\bar{x}$ be taken in the direction of the airspeed vector, along the axis of the airplane. For the effect in-the-small at any instant t_0, the wave-normals (drawn from the momentary disturbance position P_0) which are associated with the envelope will lie on a cone (not the Mach cone) defined by the angle Φ as parameter. The Mach cone, shown by dotted lines in Fig. 1 is orthogonal to these lines terminating around the circle swept over by Φ. The angle $\Phi = 0$ defines an initial direction directly under the airplane, and the pencil of lines corresponding to $-90° < \Phi < 90°$ are those initially

directed downwards. The unit wave-normal vector $\bar{\nu}$ with respect to the $(\tilde{x},\tilde{y},z)$ axes will have components

$$\begin{aligned} \tilde{p} &= 1/M \\ \tilde{q} &= -\sqrt{1 - 1/M^2}\sin\Phi \\ \tilde{r} &= -\sqrt{1 - 1/M^2}\cos\Phi \end{aligned} \tag{8}$$

Then let new axes (x,y,z) be taken with x in the direction of the ground course of the airplane. Viewed from these ground axes, it can be shown that the only effect of the wind and wind gradients in-the-small is to rotate the Mach cone axis away from the x-axis. With the components of the wind velocity vector $\bar{u}$ at the airplane denoted by $(u_x,u_y,0)$ with respect to the ground axes, the corresponding components of $\bar{\nu}$ are

$$\begin{aligned} p &= a\tilde{p} - b\tilde{q} \\ q &= b\tilde{p} + a\tilde{q} \\ r &= \tilde{r} \end{aligned} \tag{9}$$

where $b = -u_y/A$ and $a^2 = 1 - b^2$. The ground speed G is $G = aA + u_x$. The wave-normal velocity $|\bar{v}|$ for any direction $\bar{\nu}$ is given in accordance with Eq. (2) by

$$|\bar{v}| = c + \bar{u}\bar{\nu} \tag{10}$$

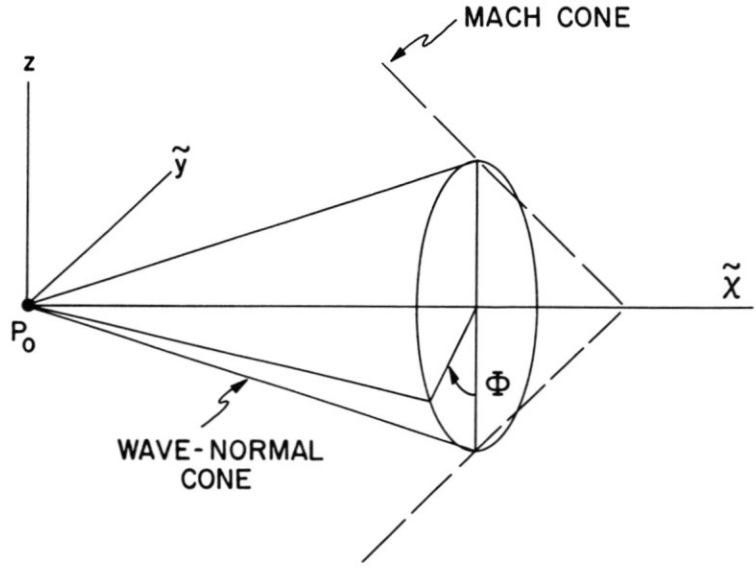

Figure 1.

The initial directions for the rays are then described by the (unnormalized) direction numbers, with respect to the ground axes,

$$\begin{aligned} R_x &= cp + u_x \\ R_y &= cq + u_y \\ R_z &= cr \end{aligned} \tag{11}$$

in accordance with Eq. (5). With the atmosphere divided into thin horizontal layers, the nth layer at the airplane height, the first calculation with Snell's law starts with $\cos \theta_n = -r$, for any fixed Φ, where θ_n is the angle of incidence of the wave-normal in the nth layer. The ray directions are next determined in terms of $\bar{\nu}_{n-1}$ in order to obtain the next interfacial position where Snell's law is again to be applied. If at any step the solution shows $\sin \theta \geqslant 1$, then calculations on that ray are stopped, since total reflection upwards has occurred.

For all of our calculations we have chosen Φ at 4° intervals between $-88° \leqslant \Phi \leqslant +88°$, thus using 45 rays per problem. By comparison with the exact solution previously mentioned, we have determined that 1,000 layers are sufficient to reduce errors to less than 0.1 percent. For many rays 100 layers are sufficient, but rays for values near $\Phi = \pm 90°$ require the finer mesh size for this accuracy.

The relative variations at ground level in overpressure at the shock front and the energy intensity available there can be determined by studying the contraction or expansion of a ray tube in the following manner.

If Δp denotes the jump in pressure across an acoustic shock, ρ the density of the basic flow, and Δu the magnitude of the jump in velocity, which is always directed normal to the wavefront, the quantity $\Delta p\ \Delta u = (\Delta p)^2/\rho c$ measures the acoustic power per unit area over the shock surface (see Ref. 11). Δp is the important quantity commonly called the "overpressure" in sonic-boom measurements.

Let us consider that the rate at which energy is supplied to the atmosphere by a particular aircraft will be a function of its airspeed and the local temperature, disregarding other parameters. Hence the acoustic power $P = f(A, T, \ldots) = P(Mc, c, \ldots)$. For our analysis M and c are held fixed. We first study two adjacent rays, separated by a small $\Delta\Phi = \Phi_{i+1} - \Phi_i$ interval, which leave the source at t_0. These strike ground at points (x_{i+1}, y_{i+1}) and (x_i, y_i). Then, after a small Δt interval, an identical ray pair will travel from the new position of the source, now displaced by a distance $G\Delta t$ in the x-direction. The area on ground enclosed by these four rays comprising the ray tube is a parallelogram with area $a = G\Delta t\,|y_{i+1} - y_i|$. The area of a normal cross section of the ray tube at ground

level is therefore equal to $-\overset{*}{R}_z a$, where $\overset{*}{R}_z$ is the (normalized) direction cosine of the ray at ground level. Along any fixed ray tube, input energy = output energy. The input energy equals $(\Delta\Phi/360)P\Delta t$, and the output is given by local energy intensity multiplied by the normal area of the tube. Let δ equal the approximately constant time required for the shock to pass a fixed point, considering now the shock to have a finite thickness. Then the energy intensity available at ground, where the wind velocity is negligible, is $\Delta p \Delta u \delta = (\delta/\rho_0 c_0)(\Delta p)^2$ where the 0 subscript refers to ground level. Hence, equating energies gives

$$\frac{\Delta\Phi}{360} P\Delta t = \frac{\delta}{\rho_0 c_0} (\Delta p)^2 (-\overset{*}{R}_z G \Delta t | y_{i+1} - y_i |) \tag{12}$$

Solving for the overpressure yields

$$\Delta p \sim \frac{\Delta\Phi}{\sqrt{-\overset{*}{R}_z G \mid y_{i+1} - y_i \mid}} \tag{13}$$

which is the fundamental quantity calculated in all our analyses of overpressure variations. The energy intensity available at the sonic-boom wavefront is proportional to $(\Delta p)^2$.

In the above we have assumed that the energy flow from the airplane to the atmosphere is nondirectional, i.e., not a function of Φ. A weighting factor could of course be inserted to include any directional behavior, but this would result in only a higher-order correction, not changing our results significantly. If we needed the actual magnitudes of the overpressure Δp at ground level, the use of inviscid linear theory throughout would not be sufficient. More precise nonlinear results or measurements would be needed to furnish the values of input energy, but for present purposes, these would constitute only superfluous initial conditions to be applied at the input of the ray tube. Also, cumulative effects of viscosity over the total ray path would require inclusion. However, this will not be significant for our comparisons since the effect largely disappears in the ratios. For the comparisons, these various refinements are not required; hence the linear acoustic theory is adequate for our purposes.

RESULTS ON THE LINEAR ATMOSPHERIC MODEL ($M = 1.5$, ALTITUDE 40,000 FEET)

For the PBB atmospheric model with linear wind velocity and linear temperature variation described above, we have calculated ray patterns and peak overpressure behavior for five wind directions with respect to the

air-speed direction. Results for one wind direction (the headwind case) are shown in Fig. 2*a*. To illustrate quantitatively effects of temperature and wind, we have included also analogous results for the simplest case (constant temperature and no winds) and for the next simplest case (the standare linear temperature variation, but no wind). This latter model causes upward reflections for all rays initially oriented for $|\Phi| > 48°$, so these rays do not reach the ground. Calculations were made at every 4th degree for Φ, but circles in Fig. 2*a* show every 10th degree, for simplicity. For the two results including both temperature and wind effects, it is seen that the PBB calculation (solid line with open circles) and our result (solid line with closed triangles) differ widely. The PBB calculations indicate reflection for $|\Phi| > 39°$, but our results indicate reflection for $|\Phi| > 7°$, and the strike positions under the airplane differ by about 35,000 ft. The two sets of results for the other four wind directions studied likewise differ considerably. For two wind directions, the PBB calculations indicated a far-field "focusing" region, but our calculations with the more exact equations failed to confirm this effect for the simple model used. Further details can be found in Ref. 10. The PBB calculations were undoubtedly correct, and we believe ours are also correct; these differences arise because we have used the exact linear acoustic theory, valid for arbitrary winds, whereas the PBB calculations were based upon the simplified Rayleigh approximation [9]. This approximation, which does not distinguish between rays and wave-normals, has been successfully used for many years for ground-level acoustic predictions connected with nuclear blasts, and is described, for example, by Cox [15]. In such applications, however, the rays are close to ground where the winds are slow, and the ray directions of interest are closer to horizontal than in sonic-boom calculations (where the winds are also very large at high altitudes). It thus appears that in sonic-boom calculations, where wind velocities are large and angles between rays and wind deviation are large, *the Rayleigh approximation for geometric acoustics is inadequate; the exact formulation which distinguishes between wave-normals and rays should be used.*

For the five wind directions which we have computed on this atmospheric model, we have found the maximum value of overpressure Δp occurring over each sonic-boom carpet. If we make a comparison with the peak Δp occurring in the "ideal" case under identical conditions, but without winds, the ratio $\mathfrak{M} = \Delta p/\Delta p_{\text{ideal}}$ represents the peak overpressure "magnification" caused by the winds. Values for this ratio are graphed in Fig. 2*b* for the five cases. One notes that the wind has little effect in reducing the ratio (minimum value is $\mathfrak{M} = 0.91$ for the tailwind case), but has considerable effect in increasing it (up to 2.21 for the headwind case). Since energy intensity varies with $(\Delta p)^2$, the maximum energy magnification is

about 4.9 times the no-wind conditions. If a probability density curve is generated from the data of Fig. 2*b*, on the basis of all directions occurring with equal probability, the result is a highly skew distribution, truncated at 0.91 and 2.21. Values on this distribution for average, median, and standard deviation of $\mathfrak{M}$ are:

$$\begin{aligned} &\text{average} && \doteq 1.23 \\ &\text{median (and no-wind case)} && = 1.00 \\ &\text{standard deviation } \sigma && \doteq 0.40 \end{aligned} \tag{14}$$

As the curve is highly nonnormal, the value of σ is not very revealing, but one sees that the average overpressure magnification for all winds is 23 percent higher than the value for the ideal no-wind atmosphere. Furthermore, all the cases (50 percent) where the $\mathfrak{M}$ is reduced lie in a small interval below the median, but the other 50 percent of the cases where $\mathfrak{M}$ is increased stretch out far above the median to a possible maximum of 2.21. These characteristics for a simple model will be compared in a later paragraph with our more general results for a very large class of statistically possible atmospheres considered globally.

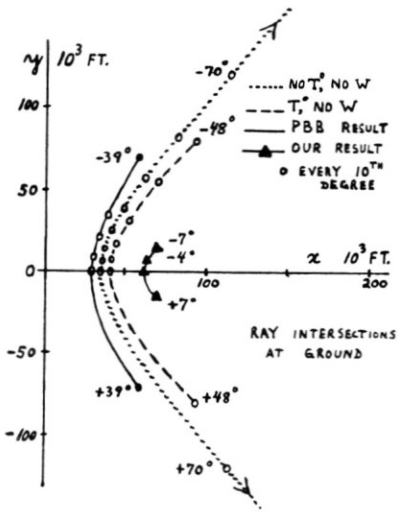

Figure 2*a*.

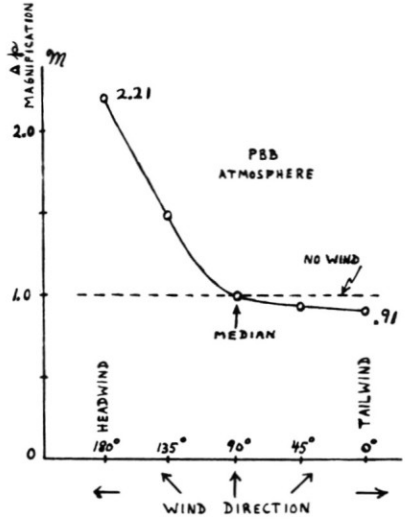

Figure 2*b*.

A REALISTIC STATISTICAL MODEL FOR GLOBAL ATMOSPHERES

Although results on simple atmospheric models such as the PBB model may reveal some essential features of sonic-boom scatter, there is nevertheless a great need for results produced by realistic complex atmospheres, encompassing the multitude of possible variations, both in-the-large and in-the-small, which do occur day by day in the earth's atmosphere, and with a relative frequency of occurrence of these variations in terms of accurate probability information. We are fortunate that such a realistic "global" atmospheric model for winds and temperatures has just recently been developed at the International Meteorological Institute in Stockholm. Although this ambitious program is still in progress, enough reliable data and processed results are now available to furnish an accurate basis for realistic sonic-boom analyses. This atmospheric investigation has been conducted over the past years by I. Holmström, and the authors express their sincere gratitude to him for his advice and active cooperation furnished in many discussions. A partial description of his method was published in 1963 (Holmström [16]). Briefly, the scheme consists in deriving from a multitude of measurements a sequence of "empirical orthogonal functions." These are used as the basis for expansions in series for various atmospheric properties. The procedure may be used for analysis of any set of data where some kind of comparatively regular behavior is expected along just one axis of the variables (here, the altitude, or equivalently the average pressure p taken as the basic independent variable). For any atmospheric property $z(p,x,y)$, a formal expansion is written

$$z(p, x, y) = \sum_{k=1}^{n} z_k(x, y)\, F_k(p) + r_n(p, x, y) \tag{15}$$

in basic functions F_k, with r_n as a remainder term. The region of interest in the atmosphere is taken as a pressure interval P from about 10 db to 1 db (ground level to about 50,000 ft, in terms of average conditions), and over an area S with dimensions comparable to a continent or larger. From thousands of measurements taken by balloon soundings over ground points (x_i, y_j) for altitudes corresponding to many pressure points p_m, the procedure consists in minimizing the variance σ_n^2 of the residual $r_n(p,x,y)$ in Eq. (15), when integrated over the total atmospheric region under consideration. This means minimization of

$$\sigma_n^2 = \frac{1}{SP} \int\int_S \int_P (z - \sum^{n} z_k F_k)^2 \, dS \, dp \tag{16}$$

for each value of $n = 1, 2, \ldots$ successively. By methods of variational calculus, a sequence of equation pairs can be obtained for the unknown functions $[F_1(p), z_1(x,y)]$, $[F_2, z_2]$, ... These equations, plus a normalizing condition on the F_k, are then solved successively by an iterative numerical method using the thousands of data points of the original measurements. The minimizing procedure leads to the orthogonal property

$$\frac{1}{P}\int_P F_k F_m \, dp = \begin{cases} 1, & k = m \\ 0, & k \neq m \end{cases} \tag{17}$$

and also assures that the "empirical orthogonal functions" $F_k(p)$ will produce the fastest possible convergence for describing possible atmospheric states. For any fixed k, the large set of values obtained for $z_k(x_i, y_j)$ is regarded as a set of values of a random variable, with known mean, deviation, cumulative distribution, etc. The statistical behavior of the atmosphere is thus described by the statistical behavior of the coefficients z_k in Eq. (15). A similar scheme for atmospheric description was also reported by Obukhov [17]. Our sonic-boom analysis has, however, been based upon the published and unpublished data furnished by Holmström. The data used by Holmström for calculating the empirical functions were obtained from more than 2,000 temperature and wind soundings measured on 8 days in 1959. In these measurements, continental areas have been overrepresented compared with other global areas. All expansions are made basically in terms of the pressure variable p; this is subsequently converted to altitude through use of curves for average pressure-altitude behavior.

Temperature Variations. A possible atmospheric temperature distribution can be represented as

$$T = T_0(p) + \sum_k T_k \tau_k(p) \tag{18}$$

where each random variable $\{T_k\}$ has known statistical properties. The first term $T_0(p)$ represents the overall average obtained, and is thus the distribution for a "standard atmosphere." Its behavior is shown as the central line labeled T_0 in Fig. 3*a*. The vertical scale is in terms of average pressure, and corresponds to altitudes from ground level to 50,000 ft. The first three orthogonal temperature functions $\tau_1(p)$, $\tau_2(p)$, and $\tau_3(p)$ are displayed in Fig. 3*b*. The remaining six lines in Fig. 3*a* illustrate how a specific distribution may be built up about T_0 using τ_1 and τ_2. These six curves represent $T_0 \pm 12\tau_1 \pm 3\tau_2$ where 12 and 3 correspond approximately to specific values of the random variables $\{T_1\}$ and $\{T_2\}$, respectively, which are equal to their standard deviations. We have not used

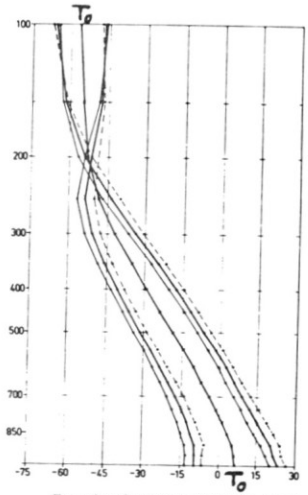

Examples of temperature profiles, taking the standard atmosphere and first and second mode successively into account.

Figure 3*a*.

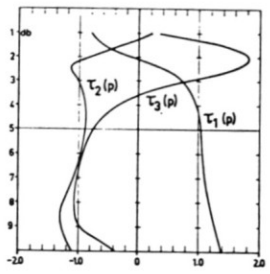

Figure 3*b*.

EMPIRICAL ORTHOGONAL FUNCTIONS OF THE ATMOSPHERE

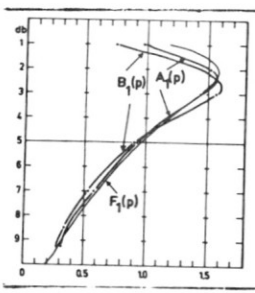

Figure 3*c*.

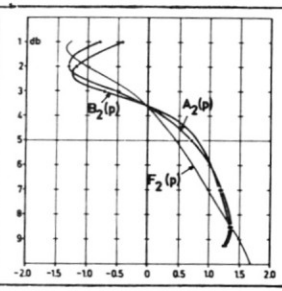

Figure 3*d*.

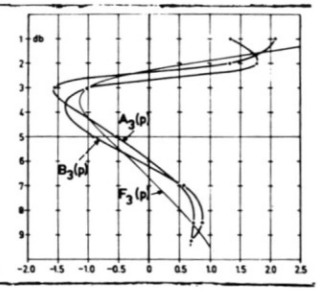

Figure 3*e*.

higher-order terms such as τ_4, τ_5, . . . because the data were not yet sufficiently complete for their precise definition. The first three terms, however, are altogether sufficient to describe the gross temperature effects for the atmosphere, but local variations, such as the familiar temperature inversion at Los Angeles, would require inclusion of 4th, 5th, or more terms for precise statistical description.

We have first tested Holmström's statistical coefficients for individual days: Within the maximum and minimum values actually measured, the distributions are very nearly normal and can safely be taken as truncated normal distribution for computational purposes.

Winds. For the general (horizontal) wind velocity vector $\overline{W} = (u,v)$, where $+u$ measures a west-to-east velocity, and $+v$ a south-to-north velocity, the wind representations are

$$u = \sum_k u_k A_k(p), \qquad v = \sum v_k B_k(p) \tag{19}$$

The orthogonal functions A_k and B_k for the first three terms are in Fig. 3*c*, *d*, and *e*. These graphs in Fig. 3 are reproduced from Ref. 16 by permission of the Tellus Journal and the author. (The F_k functions appearing in these graphs are not significant for our present application.)

We have chosen 50,000 ft as the fixed altitude for our analysis because the atmospheric data are thus far not complete for greater heights. Figure 3*c* shows that the average basic wind behavior is essentially unchanged (almost linear) up to about 40,000 ft, but then changes swiftly to a new regime above. Thus, any gross differences in final results should occur only between the ranges above-and-below 40,000 ft. This means that the general behavior of sonic-boom scattering for 50,000 ft may be extrapolated to 60,000 ft, but such would not necessarily be the case if extrapolations were attempted from results below 40,000 ft.

MONTE-CARLO GENERATION OF ATMOSPHERES

Using the known values for mean, deviation, and upper and lower bounds of the nine quantities T_1, T_2, T_3, u_1, u_2, u_3, v_1, v_2, v_3, we first generate for each model nine random numbers in the [0,1] interval. The corresponding points on the cumulative distribution curves for the nine statistical quantities given above then determine the coefficient in the expansions (18) and (19). For convenience, the distribution curves have been taken as normal, but have been truncated to be consistent with the maximum and minimum values actually measured. In this way we avoid the remote possibility of ever generating a model beyond the limits of realistic significance. Due to the presence of prevailing winds, the means for the wind coefficients are

nonzero, e.g., $u_{1\text{mean}} = 10.5$, $\sigma = 9.0$; $v_{1\text{mean}} = -1.36$, in m/sec. We have also computed the correlation coefficients ρ, and find that $\rho(u_1,v_1) = -0.05$, $\rho(u_2,v_2) = 0.18$, $\rho(u_3,v_3) = 0.16$. These values are sufficiently small so the correlations can be ignored in generating the models.

The total time needed on the computer to generate the random model, calculate 45 rays, locate the value and position of peak overpressure, and process the results is less than $1\frac{1}{2}$ minutes per atmosphere. We have computed 480 cases covering with equal probability all flight directions relative to the winds. This represents about 11 hours running time on the 7090 computer of the Swedish Air Force.

The quantity of primary interest is the magnification $\mathfrak{M}_j$ of the peak overpressure Δp for the jth atmosphere compared with the peak value for an ideal no-wind case with standard atmosphere temperature distribution or for some average or median case. Calling $Q = -\bar{R}_z G|y_{i+1} - y_i|$ from Eq. (13), where the position y has been chosen where the peak overpressure occurs, then

$$\mathfrak{M}_j = \frac{\Delta p_j}{\Delta_{p\,\text{ideal}}} = \left[\frac{Q_j}{Q_{\text{ideal}}}\right]^{-1/2}$$

The magnification can, in principle, vary beyond 1 without limit, but below 1 it can range only down to zero. We therefore make the distribution less unsymmetrical by considering the logarithm:

$$\log \mathfrak{M}_j = -\tfrac{1}{2}\log Q_j + \tfrac{1}{2}\log Q_{\text{ideal}} \equiv A_j + C \tag{20}$$

and investigate the distribution of the random variable $\{A_j\}$. The constant C causes merely a shift in the axis and has no statistical significance.

GENERAL RESULTS FOR $M = 2.2$ AND 50,000 FEET

Scatter in Overpressure. Figure 4*a* shows the computed mean of the A_i values as a function of number of cases computed. It is seen that our total of 480 cases is more than sufficient to produce a stable limiting value:

$$A_{\text{mean}} \doteq -0.40 \tag{21}$$

Figure 4*b* shows the standard deviation of the A_i's and also indicates that 480 cases are sufficient for a reasonable approximation:

$$\sigma_A \doteq 0.053 \tag{22}$$

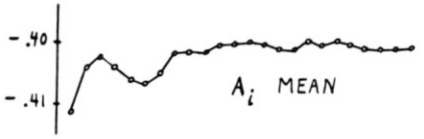

Figure 4*a*.

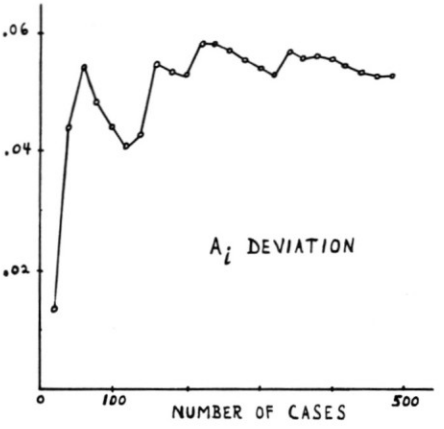

Figure 4*b*.

Figure 4*c*.

Figure 4*c* is the probability density diagram for the peak overpressure magnification in terms of the A_i variable. Its median value is

$$A_{\text{median}} = -0.4154 \tag{23a}$$

which is displaced from the mean due to the skew shape. We have also computed the "ideal" case for no-winds with only the standard atmosphere temperature T_0. Its peak, directly beneath the airplane, has for its value of overpressure magnification, in terms of the quantity A,

$$A_{\text{ideal}} = -0.4159 \tag{23b}$$

which is almost exactly our computed median value (23*a*). This shows a behavior identical with out results on the PBB model (14), and indicates that the median, not the mean, is the appropriate basis for comparisons of wind effects versus no-wind conditions. Just as in our results (14) on the PBB model, all the cases below the median lie close to it, but the remaining 50 percent of cases where $\mathfrak{M}$ is greater than 1 (compared with the median case) cover a large interval above the median. The standard deviation is thus not an accurate measure of the distribution for $\mathfrak{M} > 1$. This shape also gives the mean a higher value than the median, similar to our PBB results (14). The major portion of the distribution ranges from $A = -0.43$ to -0.30. Beyond this there are 17 cases stretching up to $A = +0.055$. Again choosing the median case as our reference for $\mathfrak{M}$, and converting from logarithms to the actual overpressure magnification, the results are:

$\mathfrak{M}$	Fraction of Total Cases Exceeding $\mathfrak{M}$
0.96	1.00
1.00	0.50
1.10	0.12
1.20	0.06
1.50	0.023
1.85	0.011
2.27	0.006
2.95	0.002

One notes that the peak value obtained ($\mathfrak{M} = 2.96$) in these 480 random cases compares closely with the peak obtained ($\mathfrak{M} = 2.21$) in our calculations on the PBB model atmosphere.

Scatter in Strike Positions. For each sonic-boom carpet computed, we have selected the point $(\hat{x},\hat{y})$ where the peak overpressure occurs. The value $|\hat{y}|$ measures the ground distance from the flight path to the line of maximum intensity. The standard deviation of these distances reaches a stable limit at 480 cases, which is

$$\sigma_{\hat{y}} \doteq 30{,}000 \text{ ft} \tag{24}$$

The probability density diagram for the quantity $|\hat{y}_j|$ has the following behavior: The values between 0 and 10,000 ft follow closely a normal curve, but the remaining 20 percent of the cases lie stretched over a wide interval from 45,000 ft up to about 100,000 ft. Thus *20 percent of the boom peaks strike outside a band about 17 miles wide beneath the airplane.*

CONCLUSIONS

We have not yet had time to make a detailed study of individual cases with very large $\mathfrak{M}$ and cases with large $|\hat{y}|$, but a cursory inspection indicates that a large part of the $\mathfrak{M}$ cases are coupled with the large $|\hat{y}|$ values. These high values of $\mathfrak{M}$ in the far-field may be caused by a shrinking together of the adjacent rays making the quantity $|\hat{y}_{i+1} - \hat{y}_i|$ small in Eq. (13), or by a reduction to very low values of the ray direction cosine $\overset{*}{R}_z$ in (13). If the latter possibility occurs in some cases, this would mean that larger overpressures are associated with "grazing" phenomena in the far-field. Because of our use of a coarse 4°-mesh for the initial ray angles $\overset{*}{\Phi}$, it is quite possible that some of these calculated $\mathfrak{M}$'s are too high; if $\overset{*}{R}_z$ goes rapidly to zero, a much finer $\Delta\Phi$ interval may be required to evaluate accurately the Δp at the grazing-zone frontier. However, there are so many cases of large $\mathfrak{M}$ and large $|\hat{y}|$ that it is likely that many have been accurately evaluated even using the large 4°-intervals. These results would then indicate some kind of strong magnification in the far-field. The point still needs detailed study, but the computing time with small $\Delta\Phi$ meshes may become so long that economic limitations might soon prevail. At present, we can only state the present results which follow necessarily from the choice of 4°-intervals. In any case, our results on scatter outside the grazing zone must be conservative, since we have taken only three terms in the wind and temperature expansions, and have not considered rays initially directed upwards, $|\Phi| > 90°$, which may reach ground and cause large overpressures.

The results, even if only partly confirmed by further study, show a scatter in overpressure intensities and in strike locations both sufficiently large to cause some concern regarding the sonic-boom menace associated with widespread supersonic commercial transportation.

The authors express their gratitude to Dr. B. K. Lundberg for initial suggestions to undertake this study and continuing advice, and to Dr. G. Drougge and Professor B. Bolin for their cooperation and valuable suggestions.

REFERENCES

1. Rao, P. S., *Aero. Quart.*, vol. 7 (February 1956 and May 1956).
2. Randall, D. G., Aeronautical Research Council, Ministry of Supply, London, R. and M. No. 3113 (1959).
3. Lansing, D. L., Symposium on Atmospheric Acoustic Propagation, El Paso, Texas (June 1961).
4. Warren, C. H. E., ICAS, IV, Paris (August 1964).
5. Lundberg, B. K. O., Memo, "Scatter in Boom Intensities," Aeronautical Research Institute, Stockholm, FFAP-GD-155 (May 1963).
6. Reed, J. W., Sandia Corp. Res. Report SC-4634, Albuquerque, N. M. (December 1961).
7. Reed, J. W., *J. Appl. Meteorol.*, vol. 1, no. 2 (June 1962).
8. Reed, J. W., and K. G. Adams, *Aerospace Eng.* (March 1962).
9. Rayleigh, Lord, *Theory of Sound* (1894), vol. 2 (New York: Dover, 1945), pp. 132-133.
10. Dressler, R. F., Publ. No. 97, Aeronautical Research Institute, Stockholm (1963).
11. Keller, J. B., *J. Appl. Phys.* (August 1954).
12. Courant-Hilbert, *Methods of Math. Physics*, vol. 2, sec. II (New York: Interscience, 1962).
13. Milne, E. A., *Phil. Mag.*, vol. 42 (July 1921).
14. Warren, C. H. E., and D. G. Randall, *Progress in Aeronautical Sciences* (New York: Pergamon, 1961), chap. 7.
15. Cox, E. F., *Handbuch der Physik*, vol. 48 (Berlin: Springer, 1958), chap. 22.
16. Holmström, I., *Tellus Journal*, XV, 2, Stockholm (1963).
17. Obukhov, A. M., *Izvestiya Geophys. Ser.* (1960), pp. 288-291.

COMMENTARY

J. P. GUIRAUD (*O.N.E.R.A., Chatillon-sur-Bagneux, Seine, France*): Je me semble que l'acoustique géométrique de J. B. Keller est une théorie de la propagation des "chocs acoustiques" et non pas une théorie de la propagation des chocs faibles. Si faible que soit un choc, sa propagation est un phènoméne non linéaire. En fait les équations de l'acoustique tolèrent des solutions discontinues, en présentant éventuellement une masse concentrée (du type de Dirac) sur une surface d'onde, et l'acoustique géométrique prévoit l'évolution de l'amplitude de cette

discontinuité, ou de cette masse concentrée, lorsque l'on se déplace le long d'un rayon sonore. Il y a plus, l'acoustique géométrique prévoit, en fait, l'évolution d'un train d'ondes, étalées autoue d'une surface d'onde, dont la largeur est trés faible en comparaison de la longueur parcourre le long du rayon sonore. On trouve que la forme du train, ou, comme l'on dit, le signal, est arbitraire, mais que l'amplitude varie selon les lois de 'l acoustique géométrique. Naturellement si l'on veut prédire l'évolution d' un tel train, même s'il est de faible amplitude, compte tenir des effets de convection non linéaires, il y a lieu de modifier l'acoustique géométrique à la maniere indiquée par Lighthill dans son article dans le volume jubilaire de G. I. Taylor.